Journal of Magnetic Resonance 214 (2012) 263–272

Contents lists available at SciVerse ScienceDirect

Journal of Magnetic Resonance

journal homepage: www.elsevier.com/locate/jmr

The time dependent Dirac–Frenkel–McLachlan variation of parameters: An NMR application

V. Lim, M.P. Augustine *

Department of Chemistry, One Shields Avenue, University of California, Davis, CA 95616, United States

ARTICLE INFO

Article history:
Received 15 July 2011
Revised 3 November 2011
Available online 7 December 2011

Keywords:
Variation of parameters
Time dependent Hamiltonian
Diffusion

ABSTRACT

The time dependent variation of parameters solution to the time dependent Schrödinger equation pioneered by Dirac, Frenkel, and McLachlan is described in terms useful for immediate application to complex time dependent problems in magnetic resonance. A benchmark comparison of the theory to one dimensional images and spin echo envelope signals in simple spatially varying magnetic fields with molecular diffusion is provided.

1. Introduction

The simulation and calculation of time domain transient signals or frequency domain spectra is central to nuclear magnetic resonance (NMR) spectroscopy [1]. Whether externally controlled pulse sequences, sample rotation in solids, or the inherent molecular dynamics in fluids or gases are present, some form of calculation is typically required to understand the resulting NMR measurements [2–4]. Theoretical modeling in NMR spectroscopy need not be complicated and involved. The motion of a single isochromatic vector according to the Bloch equations [5] and the evolution of the product operators [6] when two spins are involved are two straightforward approaches that are central to understanding the generation, evolution, and detection of NMR signals. In some cases, like the continuous averaging in solids due to magic angle spinning or the application of discontinuous and cyclic rf pulse sequences, Floquet [7,8], and average Hamiltonian [9] theories have been respectively developed to aid in the physical understanding of the spectral impact of the averaging or the removal of the non-secular contributions to the full nuclear spin Hamiltonian. Inherently adiabatic problems or those firmly embedded in the opposite sudden regime are two limits easily addressed by the Van Vleck transformation [10,11]. Whether a continuous, a discontinuous, periodic and cyclic, or an adiabatic or sudden perturbation to a large isotropic portion of the static spin Hamiltonian is accomplished, Floquet, average Hamiltonian, and the Van Vleck transformation all do remarkably well at describing measured spectra. The description of experiments in clear physical terms offered by these approximation techniques is only possible when a theory amenable to the inherent time dependence in the Hamiltonian is used and when all aspects of the time dependence i.e. the amplitude, frequency, and phase insure that the time variation is a small perturbation. If these two requirements are not guaranteed or several interfering time dependencies are present then a different theory more amenable to the time dependence must be used. Examples include multi-modal Floquet theory [12] or making the time independent part of the nuclear spin Hamiltonian a perturbation on the time dependent portion. Unfortunately in these more challenging situations traditional semi-analytical theories break down and direct numerical solutions to the Schrödinger equation, Liouville von Neumann equation, or Bloch equation must be generated [13].

The purpose of this manuscript is to introduce, develop, and demonstrate the application of the Dirac–Frenkel–McLachlan (DFM) time dependent variation of parameters [14–17] approach to an NMR problem. Although never explicitly used in the treatment of time domain NMR problems to date, the DFM approach has successfully predicted the dynamics of optically prepared wave packets on excited state molecular energy surfaces [17,18]. Unlike the Floquet, average Hamiltonian, and Van Vleck transformation methods mentioned above, the DFM approach is not restricted by either the size or symmetry of the time domain perturbation. A particularly attractive feature of the DFM method is that measured data can be used to motivate a parameterized trial function choice and that the DFM theory provides the machinery to calculate the optimum, minimum error choices for these parameters [18]. Even with optimized parameters a poor parameterized trial function will lead to a poor match with real experiments. For example, application of the DFM approach to a time dependent problem described by a time dependent Hamiltonian with characteristic

* Corresponding author. Fax: +1 530 752 8995.
E-mail address: augustin@chem.ucdavis.edu (M.P. Augustine).

1090-7807/$ - see front matter © 2011 Elsevier Inc. All rights reserved.
doi:10.1016/j.jmr.2011.11.017

frequency ω in Liouville space with the $|\rho(t)) = \sum_n |\rho_n(t))e^{in\omega t}$ trial function choice and the $|\rho_n(t))$ variable parameters automatically generates Floquet theory. Application of the Floquet approach to a discontinuous time domain problem leads to many Fourier coefficients and an intractable problem, but the alternative use of average Hamiltonian theory yields useful results. In other words, simulation ease and impact is best realized by initially choosing a trial function that adequately and accurately resembles the measured data.

There are many NMR problems available to demonstrate the application of the DFM variation of parameters: spin diffusion in solids [19], heteronuclear decoupling during magic angle spinning in solids [20], cross polarization in rotating solids [21], radiation damping and feedback in inhomogeneously broadened systems [22], classical diffusion in an rf gradient in the presence of chemical shifts and or scalar, dipolar, or quadrupolar couplings [23], etc. To develop the DFM variation of parameters for NMR problems a simple application where experimental data is immediately available was chosen to evaluate the performance of the theoretical approach. Experimental free precession signals for long and reduced volume samples of water in one dimensional linear and quadratic shaped magnetic fields applied parallel to the applied static magnetic field are reproduced with the DFM theory. The DFM simulations use available molecular and hardware dependent parameters such as diffusion constants and pulse sequence characteristics. The particular choice of the treatment of translational molecular motion was motivated by the availability of a solution to the problem generated by Hahn for the case of diffusion in a linear field [24]. In this way, the DFM modeling of the linear field free precession and spin echo signals serves as a benchmark comparison to existing theory while the evolution of spin magnetization in the yet to be solved quadratic shaped magnetic field and mixed linear and quadratic fields is new and will be described below.

The next section describes how to apply the DFM variation of parameters to NMR problems for the case of molecular diffusion in a linear and quadratic shaped field. Following this introduction, a brief experimental section describing the NMR instrument and samples is provided. Finally the theory is applied to the modeling of experimental data.

2. Theory

It is important to realize throughout this section that the DFM variation of parameters is completely general and can be applied to any time dependent differential equation. In addition, it provides the machinery to optimize any trial function guess for the observable signal, density operator element, or magnetization and provides an internal self-contained estimate of the quality of the trial function guess.

2.1. The DFM variation of parameters

A starting point for the application of the DFM theory to the problem of diffusion in a linear and quadratic magnetic field is the Bloch–Torrey equation [25]

$$\frac{\partial}{\partial t}\vec{M}(t) = \gamma \vec{M}(t) \times \vec{H} + D\nabla^2 \vec{M}(t) - \Gamma(\vec{M}(t) - \vec{M}_{eq}) \tag{1}$$

where $\vec{M}(t)$ is the classical x, y, z, and t spatially and time dependent magnetization, H is the applied magnetic field, ∇^2 is the Laplacian operator, Γ is the relaxation matrix, γ is the gyromagnetic ratio, D is the diffusion coefficient, and $\vec{M}_{eq} = (N\hbar\omega_0/kT)\hat{z}$ is the thermal equilibrium magnetization written in terms of the number of spins N, Planck's constant $\hbar$, Boltzmann's constant k, temperature T, the Larmor frequency $\omega_0 = \gamma H$, and the direction of the applied static magnetic field $\hat{z}$. The first step of the DFM variation of parameters is to define a functional for $\vec{M}(t)$ or a function of Eq. (1) that is zero valued when the correct trial function for the magnetization $\vec{M}(t)$ is identified, non-zero valued in the limit of an inaccurate trial function, and larger valued for increasingly poor choices of the trial function used for $\vec{M}(t)$. Although there is an arguable infinite number of functional guesses that meet these criteria, the simplest and most consistent with the original DFM work [17,18] is

$$T(\vec{M}(t), \partial\vec{M}(t)/\partial t) = \int \left| \frac{\partial}{\partial t}\vec{M}(t) - \gamma \vec{M}(t) \times \vec{H} + D\nabla^2 \vec{M}(t) - \Gamma(\vec{M}(t) - \vec{M}_{eq}) \right|^2 dV \tag{2}$$

where the integral is performed over the volume element dV.

As written, Eq. (1) anticipates that the dependent variables in the magnetization are space (x, y, z), (r, θ, ϕ), or volume V and time. However in addition to this inherent spatial and temporal dependence $\vec{M}(t)$ can also be considered a function of a set of $n+1$ time dependent variable parameters $\{\xi_n(t)\} = \{\xi_0(t), \xi_1(t), \xi_2(t), \ldots, \xi_n(t)\}$. In direct analogy to the DFM theory [17,18], the variation of $T(\vec{M}(t), \partial\vec{M}(t)/\partial t)$ in Eq. (2) with respect to the variation in $\partial\vec{M}(t)/\partial t$ yields

$$\delta T_p = 0 = \int \left(\frac{\partial \vec{M}(\{\xi_n(t)\})}{\partial \xi_p} \right)^{\dagger} \cdot \left[\frac{\partial}{\partial t}\vec{M}(\{\xi_n(t)\}) - \gamma \vec{M}(\{\xi_n(t)\}) \times \vec{H} - D\nabla^2 \vec{M}(\{\xi_n(t)\}) + \Gamma(\vec{M}(\{\xi_n(t)\}) - \vec{M}_{eq}) \right] dV \tag{3}$$

for $p = 0, 1, 2 \ldots n+1$. Simultaneously solving the $n+1$ equations will determine each parameter in the $\{\xi_n(t)\}$ set. The $\xi_n(t)$ functions correspond to the parameters that yield the best agreement of the trial function $\vec{M}(\{\xi_n(t)\})$ with the true solution to Eq. (1).

Both Eqs. (2) and (3) are expressed in terms of the real spatial coordinates assigned by the direction of the applied field H. However, since a trial magnetization function is parameterized as $\vec{M}(\{\xi_n(t)\})$, the problem reduces to the determination of the time dependence of the $\{\xi_n(t)\}$ parameters. It is more natural to instead write Eqs. (2) and (3) in terms of the parameter vector $\vec{\xi}(t) = \sum_{p=0}^{n} \xi_p(t)\hat{\xi}_p$ where the $n+1$ time independent unit vectors $\hat{\xi}_p$ correspond to the $n+1$ separate orthogonal directions in an $(n+1) \times (n+1)$ dimensional parameter space. This definition of the parameter vector along with the realization that $\partial\vec{M}(\{\xi_n(t)\})/\partial t = \sum_{p=0}^{n} (\partial\vec{M}(\{\xi_n(t)\})/\partial\xi_p(t)) \cdot (d\xi_p(t)/dt)$ allows Eq. (3) to be rewritten as

$$\underset{\sim}{A} \cdot \frac{d\vec{\xi}(t)}{dt} = \vec{B} \tag{4}$$

where the elements of the column vector $d\vec{\xi}(t)/dt$ are the appropriate $d\xi_n(t)/dt$ time derivatives. The elements of the matrix $\underset{\sim}{A}$ are

$$A_{r,p} = \int \left(\frac{\partial \vec{M}(\{\xi_n(t)\})}{\partial \xi_p(t)} \right)^{\dagger} \cdot \left(\frac{\partial \vec{M}(\{\xi_n(t)\})}{\partial \xi_r(t)} \right) dV \tag{5}$$

and the elements of the vector $\vec{B}$ are

$$B_p = \int \left(\frac{\partial \vec{M}(\{\xi_n(t)\})}{\partial \xi_p(t)} \right)^{\dagger} \cdot \left[\gamma \vec{M}(\{\xi_n(t)\}) \times \vec{H} + D\nabla^2 \vec{M}(\{\xi_n(t)\}) - \hat{\Gamma}(\vec{M}(\{\xi_n(t)\}) - \vec{M}_{eq}) \right] dV \tag{6}$$

in Eq. (4). Eqs. (2) and (4) are used in tandem to evaluate the quality of the trial function $\vec{M}(\{\xi_n(t)\})$ and to calculate the values of the

$\{\xi_n(t)\}$ parameters that provide the lowest possible value for $T(\vec{M}(t), \partial\vec{M}(t)/\partial t)$. The solution for $\vec{\xi}(t)$ obtained from Eq. (4) is used to determine of $\vec{M}(\{\xi_n(t)\})$ as a function of time. The next section simplifies the above expressions by considering actual experimental conditions and subsequent sections describe one way to apply the method to experiments.

2.2. Reduction to the experimental case

The case of one dimensional diffusion in a linear and/or quadratic shaped magnetic field considered here is much simpler than the three dimensional situation described above. The Laplacian reduces to one dimension and the time scale of the experiment permits spin–lattice relaxation effects and thus the effect of $\vec{M}_{eq}$ to be negligible. Transverse relaxation effects are still present although the relaxation matrix Γ reduces to the $1/T_2$ scalar value. In this limit, the time evolution of the complex transverse magnetization $M_+(t) = M_x(t) + iM_y(t)$ in the rotating frame magnetic field $\vec{H} = (Gz + Kz^2)\hat{z}$ described by the field gradient G and its derivative K reduce Eq. (1) to

$$\frac{\partial}{\partial t}M_+(t) = \left(D\frac{\partial^2}{\partial z^2} - i\gamma Gz - i\gamma Kz^2 - \frac{1}{T_2}\right)M_+(t) \tag{7}$$

and Eq. (2) to

$$T(\vec{M}_+(t), \partial\vec{M}_+(t)/\partial t) = \int \left|\frac{\partial}{\partial t}\vec{M}_+(t) - \left(D\frac{\partial^2}{\partial z^2} - i\gamma Gz - i\gamma Kz^2 - \frac{1}{T_2}\right)M_+(t)\right|^2 dz \tag{8}$$

As with the general case, Eqs. (7) and (8) can be used to deduce the elements of the matrix $\tilde{A}$ as

$$A_{r,p} = \int \left(\frac{\partial M_+(\{\xi_n(t)\})}{\partial \xi_p(t)}\right)^\dagger \cdot \left(\frac{\partial M_+(\{\xi_n(t)\})}{\partial \xi_r(t)}\right) dz \tag{9}$$

and the elements of the vector $\vec{B}$ as

$$B_p = \int \left(\frac{\partial M_+(\{\xi_n(t)\})}{\partial \xi_p}\right)^\dagger \cdot \left(D\frac{\partial^2}{\partial z^2} - i\gamma Gz - i\gamma Kz^2 - \frac{1}{T_2}\right)M_+(\{\xi_n(t)\})dz \tag{10}$$

Eqs. (9) and (10) are needed to determine the time evolution of the $\{\xi_n(t)\}$ parameter set from the solution to Eq. (4). The quality of the trial function solution to Eq. (7) in terms of the optimized set of functions $\{\xi_n(t)\}$ is assessed from the functional $T(\vec{M}(t), \partial\vec{M}(t)/\partial t)$ defined by Eq. (8).

2.3. Single Gaussian solution

The success enjoyed by Heller in the choice of a parameterized Gaussian wave function to describe the evolution of coherences in a wave packet translating on an excited state energy surface [17,18] prompts the application of the three parameter Gaussian trial magnetization

$$M_+^G(\{\xi_2(t)\}) = M_0 e^{-\xi_2(t)z^2 - \xi_1(t)z - \xi_0(t)} \tag{11}$$

where $M_0 = \vec{M}_{eq}\cdot\hat{k}$. An attractive feature of the choice of a Gaussian trial magnetization $M_+^G(\{\xi_2(t)\})$ is that all of the elements of the matrix $\tilde{A}$ and the vector $\vec{B}$ shown in Eqs. (9) and (10) respectively can be analytically determined regardless of the fundamental constants e.g. D, G, K, T_2 used and of the time t. Using Eq. (11) with Eq. (4) yields

$$\begin{aligned}
\frac{d}{dt}\xi_2(t) &= -4D\xi_2(t)^2 + iK \\
\frac{d}{dt}\xi_1(t) &= -4D\xi_1(t)\xi_2(t) + iG \\
\frac{d}{dt}\xi_0(t) &= 2D\xi_2(t) - D\xi_1(t)^2 + \frac{1}{T_2}
\end{aligned} \tag{12}$$

Inserting the solution to these equations into the definition for $M_+^G(\{\xi_2(t)\})$ in Eq. (11) followed by calculation of the value of the functional in Eq. (8) yields $T(\vec{M}(t), \partial\vec{M}(t)/\partial t) = 0$. This implies that as long as Eqs. (12) are solved, $M_+^G(\{\xi_2(t)\})$ is an exact solution to the Bloch Eq. (7).

2.3.1. Homogeneous rf pulses

The appropriateness of the $M_+^G(\{\xi_2(t)\})$ trial magnetization to the solution of the Bloch Eq. (7) is captured by the value of the $\xi_n(0)$ parameters. As long as the initial magnetization is Gaussian distributed symmetrically (or in a completely anti-symmetric fashion) about $z = 0$ the DFM variation of parameters with the $M_+^G(\{\xi_2(t)\})$ trial magnetization produces the true spatial and temporal development of the magnetization. The parameter values at $t = 0$ specify the magnetization distribution immediately following a $\pi/2$ rf pulse. In the case where there is no rf inhomogeneity and the sample is small and contained within the rf excitation coil, $\xi_0(0) = \xi_1(0) = \xi_2(0) = 0$ and the magnetization is uniformly excited. The solutions to Eq. (12) with these initial conditions provide the optimized $\xi_n(t)$ parameters needed to calculate $M_+^G(\{\xi_2(t)\})$ in Eq. (11). The free precession signal $S(t)$ is the integral of $M_+^G(\{\xi_2(t)\})$ over the dimensions or the length L of the sample as

$$S(t) = \int_{-L/2}^{L/2} M_+^G(\{\xi_2(t)\})dz = \int_{-\infty}^{+\infty} M_+^G(\{\xi_2(t)\})g(z)dz \tag{13}$$

where $g(z) = 1$ for $-L/2 \leqslant z \leqslant L/2$ and $g(z) = 0$ elsewhere. The effects of the $\pi/2$–τ–π spin echo pulse sequence can also be treated with this variational approach. Application of a π rf pulse at the time $t = \tau$ after the $\pi/2$ rf pulse essentially exchanges the complex components of the magnetization with each other. Specifically, a π rf pulse elicits the transformation $M_+ \rightarrow M_-$ and vice versa. This means that the solutions to Eq. (12) also describe the spatial and temporal evolution of the spin echo magnetization. This is true as long as the new initial parameter values immediately after the π rf pulse at the time $t = \tau = 0_+$ are appropriately related to the parameter values at the time $t = \tau$ before the π rf pulse as $\xi_n(0_+) = \xi_n(\tau)^*$. Application of the spatially abbreviated integral in Eq. (13) to the $M_+^G(\{\xi_2(t)\})$ magnetization following the π rf pulse provides the time development of the spin echo signal, and thus an equation that can be compared to experiment.

2.3.2. Inhomogeneous rf pulses: Gaussian profile

The effects of diffusion on free precession and spin echo signals in the presence of inhomogeneous rf pulses can also be explored using the DFM variation of parameters. In order to compare theory to experiment, consider the special example of an rf coil partially enclosing an infinitely long cylindrical sample with the long axis parallel to the direction of the applied G and K fields and where the amplitude of the applied rf field behaves according to $H_1(z) = H_1(0)\exp[-\xi_2(0)z^2]$. In this case, a small tip angle inhomogeneous rf pulse yields $\xi_2(0) \neq 0$ and $\xi_1(0) = \xi_0(0) = 0$. The solutions for the $\{\xi_2(t)\}$ set of parameters from Eq. (12) with these initial conditions provides $M_+^G(\{\xi_2(t)\})$ and the free precession signal from Eq. (13) with $g(z) = H_1(z)/H_1(0)$. The functional form of the rf excitation $H_1(z)/H_1(0)$ is included as diffusion will move rf pulse excited magnetization from and thermal equilibrium magnetization into the active rf coil region of the infinitely long sample.

The $\pi/2$–τ–π spin echo signal generated from a small tip angle pulse followed by a homogenous π pulse is calculated in exactly

the same way as in the previous section. Since the π rf pulse converts M_+ into M_- and vice versa, the parameters immediately after the π rf pulse at the time $t = 0_+$ are related to the parameters immediately before the π rf pulse as $\xi_n(0_+) = \xi_n(\tau)^*$. These values are used as initial conditions to solve Eq. (12) for the $\{\xi_2(t)\}$ parameter set and ultimately the spin echo magnetization $M_+^G(\{\xi_2(t)\})$. Application of Eq. (13) with $g(z) = H_1(z)/H_1(0)$ provides the spin echo signal that can be compared to experiment.

A limitation of this approach is the neglect of the effects of rf inhomogeneity on the π rf pulse. In order to account for these effects on the spin echo magnetization and the effects of rf inhomogeneity on measured signals resulting from any multiple rf pulse sequence, a wave packet trial magnetization can be used and is described below.

2.4. Gaussian wave packet solution

The Gaussian trial magnetization in Eq. (11) adequately describes NMR signals in the presence of diffusion when small samples are used and homogeneous rf fields are applied. Additionally, the single Gaussian trial magnetization can be used to determine the free induction signals for infinitely long samples stimulated with a small tip angle rf pulse with Gaussian spatial inhomogeneity. However, the use of a single Gaussian trial magnetization is limited as the signal corresponding to multiple rf pulses and to rf pulses with non-Gaussian spatial distributions cannot be satisfactorily treated. These problems are circumvented by instead choosing a Gaussian wave packet trial magnetization [18]

$$M_+^{wp}(\{\xi_2(z_n,t)\}) = M_0 \sum_{q=0}^{n} m_+(\{\xi_2(z_q,t)\}) \tag{14}$$

written in terms of individual Gaussian magnetizations

$$m_+(\{\xi_2(z_q,t)\}) = e^{-\xi_2(z_q,t)(z-z_q)^2 - \xi_1(z_q,t)(z-z_q) - \xi_0(z_q,t)} \tag{15}$$

Each separate Gaussian $m_+(\{\xi_2(z_q,t)\})$ is centered at position z_q and is characterized by the three variational parameters $\xi_0(z_q,t)$, $\xi_1(z_q,t)$, and $\xi_2(z_q,t)$. The number of optimizable parameters increases from 3 for the single Gaussian trial magnetization shown in Eq. (11) to $3(n+1)$ for the wave packet; 3 parameters for each of the $n+1$, z_q offset Gaussian functions $m_+(\{\xi_2(z_q,t)\})$ comprising $M_+^{wp}(\{\xi_2(z_n,t)\})$. The dimensionality of the parameter vector $\vec{\xi}(t)$ concomitantly increases the dimensionality of $\underset{\sim}{A}$ and $\vec{B}$. Arranging the elements of $\vec{\xi}(t)$ in terms of the separate Gaussian basis magnetizations $m_+(\{\xi_2(z_q,t)\})$ centered at the position z_q provides the elements of the matrix $\underset{\sim}{A}$ as

$$A_{3q+r,3k+p} = \int \left(\frac{\partial m_+(\{\xi_2(z_q,t)\})}{\partial \xi_p(z_q,t)}\right)^{\dagger} \cdot \left(\frac{\partial m_+(\{\xi_2(z_k,t)\})}{\partial \xi_r(z_k,t)}\right) \mathrm{d}z \tag{16}$$

and the elements of the vector $\vec{B}$ as

$$B_{3k+p} = \int \left(\frac{\partial m_+(\{\xi_2(z_k,t)\})}{\partial \xi_p(z_k,t)}\right)^{\dagger} \cdot \left(D\frac{\partial^2}{\partial z^2} - i\gamma G z - i\gamma K z^2 - \frac{1}{T_2}\right) \sum_{q=0}^{n} m_+(\{\xi_2(z_q,t)\}) \mathrm{d}z \tag{17}$$

where the indices q and k include 0, 1, 2, …, n, while the indices q and r are limited to 0, 1, 2. Provided that Eq. (4) is exactly solved for $\vec{\xi}(t)$ or the time dependence of the $\{\xi_2(z_q,t)\}$ parameter set, the Gaussian wave packet trial magnetization $M_+^{wp}(\{\xi_2(z_n,t)\})$ exactly solves the Bloch Eq. (7). The use of a sum of Gaussian magnetization basis functions $m_+(\{\xi_2(z_q,t)\}$ used to define the wave packet reduces the $3(n+1)$ coupled equations for the $\{\xi_2(z_q,t)\}$ parameter set developed from Eq. (4) into $n+1$ sets of 3 coupled equations characterized by the specific offset displacement z_q as

$$\begin{aligned}
\frac{d}{dt}\xi_2(z_q,t) &= -4D\xi_2(z_q,t)^2 + iK \\
\frac{d}{dt}\xi_1(z_q,t) &= -4D\xi_1(z_q,t)\xi_2(z_q,t) + iG + 2iKz_q \\
\frac{d}{dt}\xi_0(z_q,t) &= 2D\xi_2(z_q,t) - D\xi_1(z_q,t)^2 + \frac{1}{T_2} + iGz_q + 2iKz_q^2
\end{aligned} \tag{18}$$

These equations are the same set of equations shown in Eq. (12) with the exception of the added offset dependent constants in the $d\vec{\xi}_0(z_q,t)/dt$ and $d\vec{\xi}_1(z_q,t)/dt$ equations. These additional constants do not prevent the straightforward analytical or numerical solution to Eq. (18) and thus the wave packet magnetization $M_+^{wp}(\{\xi_2(z_n,t)\})$ can be obtained from Eqs. (14) and (15). Proceeding in direct analogy to Sec. 2.3 for the single Gaussian solution, calculation of the functional in Eq. (8) from $M_+^{wp}(\{\xi_2(z_n,t)\})$ written in terms of the parameters optimized according to Eq. (18) again yields $T(\vec{M}(t), \partial\vec{M}(t)/\partial t) = 0$. This implies that as long as Eqs. (18) are solved, $M_+^{wp}(\{\xi_2(z_n,t)\})$ is also an exact solution to the Bloch Eq. (7).

It is important to note that the clean separation of the wave packet variation parameters into $(n+1)$ sets of 3 coupled equations in Eq. (18) is only true for a wave packet of Gaussian basis functions. It is the mathematical properties of the exponential function that leads to a factoring and reduction of the number of terms in $\underset{\sim}{A}$ and $\vec{B}$ for the wave packet magnetization. This ultimately uncouples the evaluation of the $\{\xi_2(z_n,t)\}$ set into groups of similar equations like Eq. (18).

2.4.1. Inhomogeneous rf pulses: arbitrary profile

The Gaussian wave packet solution to the Bloch equation is capable of modeling the free precession and spin echo signals generated by rf pulses of any specified inhomogeneity. To accomplish this goal the number of Gaussian basis functions $m_+(\{\xi_2(z_q,t)\})$ contributing to the total wave packet $M_+^{wp}(\{\xi_2(z_n,t)\})$, the uniform separation $\Delta z = z_{q+1} - z_q$, and the initial Gaussian basis function width $\xi_2(z_q,0)$ before the application of an rf pulse must be specified. To ensure a smooth spectral profile as a function of the real displacement z in the wave packet $M_+^{wp}(\{\xi_2(z_n,t)\})$, the initial line width $\xi_2(z_q,0)$ is limited by the coalescence point of two Gaussian functions Δz as $\xi_2(z_q,0) \leqslant 2/(\Delta z)^2$.

Application of an inhomogeneous rf pulse to thermal equilibrium magnetization in a perfectly homogeneous static magnetic field can be approximated as $M_+(z,0) = M_0 \sin[\theta(z)]$. The spatially dependent tip angle $\theta(z)$ is related to the inhomogeneous rf field as $\theta(z) = \gamma H_1(z)$. This initial spatial dependence in the actual $M_+(z,0)$ complex magnetization is incorporated into the initial $t = 0$ wave packet trial magnetization $M_+^{wp}(\{\xi_2(z_n,0)\})$ by adjusting the initial amplitude of each of the Gaussian basis functions $m_+(\{\xi_2(z_q,0)\})$, or equivalently by assigning $\xi_0(z_q,0) = -\ln(\sin[\theta(z_q)])$ in the Gaussian basis function centered at the position z_q. The free precession signal following an inhomogeneous rf pulse in the presence of diffusion is then calculated by solving for the time dependence of the $\{\xi_2(z_n,t)\}$ parameter set from Eq. (18) given that $\xi_2(z_q,0) \leqslant 2/(\Delta z)^2$, $\xi_1(z_q,0) = 0$, and $\xi_0(z_q,0) = -\ln(\sin[\theta(z_n)])$. These time dependent parameters are used to calculate the time dependence of each of the separate Gaussian basis functions $m_+(\{\xi_2(z_q,t)\})$ and ultimately the Gaussian wave packet magnetization $M_+^{wp}(\{\xi_2(z_n,t)\})$. The result can be used along with Eq. (13) to determine the free precession signal where $M_+^{wp}(\{\xi_2(z_n,0)\})$ replaces $M_+^G(\{\xi_2(t)\})$ and $g(z) = H_1(z)/H_1(0)$.

The effects of general rf inhomogeneity on the spin echo signal generated from the $\pi/2$–τ–π pulse sequence can also be treated with the Gaussian wave packet approach. Since a pair of inhomogeneous rf pulses differing in either duration or amplitude by a factor of two are used, a better representation of the spin echo pulse sequence that approximates the effect of rf inhomogeneity is $\theta(z)$–

τ–$2\theta(z)$. In the limit of a perfectly homogeneous static magnetic field, the application of a $2\theta(z)$ rf pulse to the transverse magnetization $M_{\pm}(z,\tau)$ at the time t = τ mixes the complex components into each other as

$$M_{\pm}(z,0_{+}) = \frac{1}{2}(1 \pm \cos[2\theta(z)])M_{+}(z,\tau) + \frac{1}{2}(1 \mp \cos[2\theta(z)])M_{-}(z,\tau) \quad (19)$$

Any magnetization left along the z axis from the first $\theta(z)$ rf pulse is rotated into the transverse plane by the second $2\theta(z)$ rf pulse and does not contribute to the echo signal. The spatial dependence in the real $M_{+}(z,0_{+})$ magnetization following the $2\theta(z)$ rf pulse is incorporated into the $t = 0_{+}$ wave packet trial magnetization $M_{+}^{wp}(\{\xi_2(z_n,0_{+})\})$ by separately determining the parameter set $\{\xi_2(z_n,0_{+})\}$ after the $2\theta(z)$ pulse for each of the Gaussian basis functions in terms of the respective values $\{\xi_2(z_n,\tau)\}$ prior to the $2\theta(z)$ rf pulse applied at the time $t = \tau$. Eq. (19) for the case of general rf inhomogeneity can be approximated as

$$m_{+}(\{\xi_2(z_q,0_{+})\}) = \frac{1}{2}(1 + \cos[2\theta(z_q)])m_{+}(\{\xi_2(z_q,\tau)\}) + \frac{1}{2}(1 - \cos[2\theta(z_q)])m_{-}(\{\xi_2(z_q,\tau)\}) \quad (20)$$

for each Gaussian trial function in the wave packet. The set of new parameters after the $2\theta(z)$ rf pulse $\{\xi_2(z_q,0_{+})\}$ in terms of the parameter set prior to the $2\theta(z)$ rf pulse $\{\xi_2(z_q,\tau)\}$ and the complex conjugate value $\{\xi_2(z_q,\tau)^{*}\}$ introduced by the $m_{-}(\{\xi_2(z_q,\tau)\})$ dependence in Eq. (20) is obtained by using the definition for $m_{+}(\{\xi_2(z_q,t)\})$ shown in Eq. (15) and by solving Eq. (20) for the $\{\xi_2(z_q,0_{+})\}$ values. It is these new values at the time $t = 0_{+}$ that serve as initial conditions for the determination of the $\{\xi_2(z_n,t)\}$ parameters from Eq. (18) for the spin echo magnetization $M_{+}^{wp}(\{\xi_2(z_n,t)\})$ and thus the measured signal.

3. Experimental

All NMR experiments were performed using a wide bore Oxford Instruments 6.95 T superconducting solenoid magnet. A Nalorac double resonance probe mounted in an Oxford Instruments 18 channel shim set and connected to a double resonance Tecmag Apollo pulse programmer was used to obtain all free precession and echo envelope signals in this study. A standard 5 mm outer diameter Pyrex NMR tube loaded with a 5 cm column of deionized water was used to mimic an infinitely long sample. Linear 1.4 G/cm, 2.8 G/cm, and 4.5 G/cm and quadratic 6.4 G/cm^2, 12.5 G/cm^2, and 18.8 G/cm^2 fields were established and calibrated by respectively adjusting the $z1$ and $z2$ shim currents applied to the Oxford shim set and by relating the spectral width of the Fourier transformed free precession signal to sample length for a finite 1 cm long water sample contained in a Shigemi tube centered in the rf coil. All theoretical calculations and data processing were accomplished using Mathematica.

4. Results

The DFM variation of parameters as applied to diffusion in one dimensional linear and quadratic shaped magnetic fields as described in Section 2 provides useful theoretical results that are easily compared to experiment. Analytical expressions for the spatially dependent free precession and spin echo magnetization and the concomitant signal can be developed in either linear or quadratic shaped magnetic fields. However, examples involving mixed linear and quadratic shaped magnetic fields are often not analytically tractable due to the sheer number of terms required to solve the Bloch Eq. (7). Examples where analytical results can be generated from the DFM approach considers the free precession and spin echo magnetizations and signals for a small sample of length L completely enclosed within the rf coil. Since the applied rf field in this case is perfectly homogeneous, the single Gaussian trial magnetization applies with $\xi_0(0) = \xi_1(0) = \xi_2(0) = 0$. The solution to Eq. (12) yields $\xi_0(t) = t/T_2 + (\gamma G)^2 Dt^3/3$, $\xi_1(t) = -i\gamma Gt$, and $\xi_2(t) = 0$. These parameters define the free precession magnetization as

$$M_{+}^{G}(\{\xi_2(t)\}) = M_0 e^{i\gamma Gzt - (\gamma G)^2 Dt^3/3 - t/T_2} \quad (21)$$

and the observed free precession signal as

$$S(t) = \frac{2M_0}{\gamma Gt}\sin\left(\frac{\gamma GLt}{2}\right)e^{-(\gamma G)^2 Dt^3/3 - t/T_2} \quad (22)$$

A similar analysis for the spin echo envelope signal in this example yields $\xi_0(2\tau) = 2\tau/T_2 + 2(\gamma G)2D\tau^3/3$ and $\xi_1(2\tau) = \xi_2(2\tau) = 0$ from the solution to Eq. (12). These parameters produce Hahn's famous result [24]

$$S(t) = M_{+}^{G}(\{\xi_2(2\tau)\}) = M_0 e^{-(\gamma G)^2 D 2\tau^3/3 - 2\tau/T_2} \quad (23)$$

Another situation where the DFM variation of parameters provides a useful result with a limited number of terms considers the free precession signal due to the application of a linear magnetic field to an infinitely long sample following a small tip angle rf pulse with a Gaussian spatial excitation profile. Here the solution to Eq. (12) with the $\xi_0(0) = \xi_1(0) = 0$ and $\xi_2(0) \neq 0$ initial conditions along with $\theta = \gamma H_1(0)t_p$ where t_p is the pulse length yields the free precession signal as

$$S(t) = M_0 sin(\theta)\sqrt{\frac{\pi}{2\xi_2(0)(1 + 2\xi_2(0)Dt)}}e^{\frac{-(\gamma G)^2 t^2}{8\xi_2(0)} - (\gamma G)^2 Dt^3/12 - t/T_2} \quad (24)$$

after application of Eq. (13) with $g(z) = \exp(-\xi_2(0)z^2)$.

The solid black lines for the one rf pulse spectra in Fig. 1 and the black symbols for the echo envelope signal in Fig. 2 correspond to experimental data obtained for a 5 cm long tube of water centered on the 1.6 cm long rf coil. The measured data in Figs. 1a–c and 2a–c are reproduced in Figs. 1d–f and 2d–f respectively for comparison to both the single Gaussian in Figs. 1a–c and 2a–c and the Gaussian wave packet in Figs. 1d–f and 2d–f trial functions. The three different magnetic field gradient choices of 1.4 G/cm, 2.8 G/cm, and 4.5 G/cm produce the three images of increasing width in Fig. 1a and d and the echo envelope signals corresponding to the cross, open circle, and x in Fig. 2a and d respectively. The same relationship between applied quadratic magnetic field variation and line width for the three 6.4 G/cm^2, 12.5 G/cm^2, and 18.8 G/cm^2 amplitudes yield the offset images in Fig. 1b and d and the echo envelope signals for the cross, open circle, and x in Fig. 2b and e. Experimental and computational examples of the mixed gradient case are also included in Figs. 1 and 2. Values of 1.4 G/cm and 12.5 G/cm^2 were used to generate the lower image in Fig. 1c and f while the offset images in Fig. 1c and f were obtained with a 2.8 G/cm and 18.8 G/cm^2 linear and quadratic field values. The echo envelope signals shown in Fig. 2c and f all correspond to the application of a 1.4 G/cm linear magnetic field variation while the quadratic field value increases as 6.4 G/cm^2, 12.5 G/cm^2, and 18.8 G/cm^2 for the cross, open circle and x symbol respectively. The light gray lines shown in Fig. 1a–c correspond to the signals calculated from the single Gaussian trial magnetization $M_{+}^{G}(\{\xi_2(t)\})$ with $D = 2.2 \times 10^{-5}$ cm^2/s, $T_2 = 2.6$ s, the appropriate applied magnetic field variation amplitudes, $\xi_0(0) = \xi_1(0) = 0$, and $\xi_2(0) = 0.6$ cm^{-2} as estimated by tracking the spectral intensity for a small droplet of water translated through the rf coil along the z axis. The same constant values were used to generate the light gray curves shown

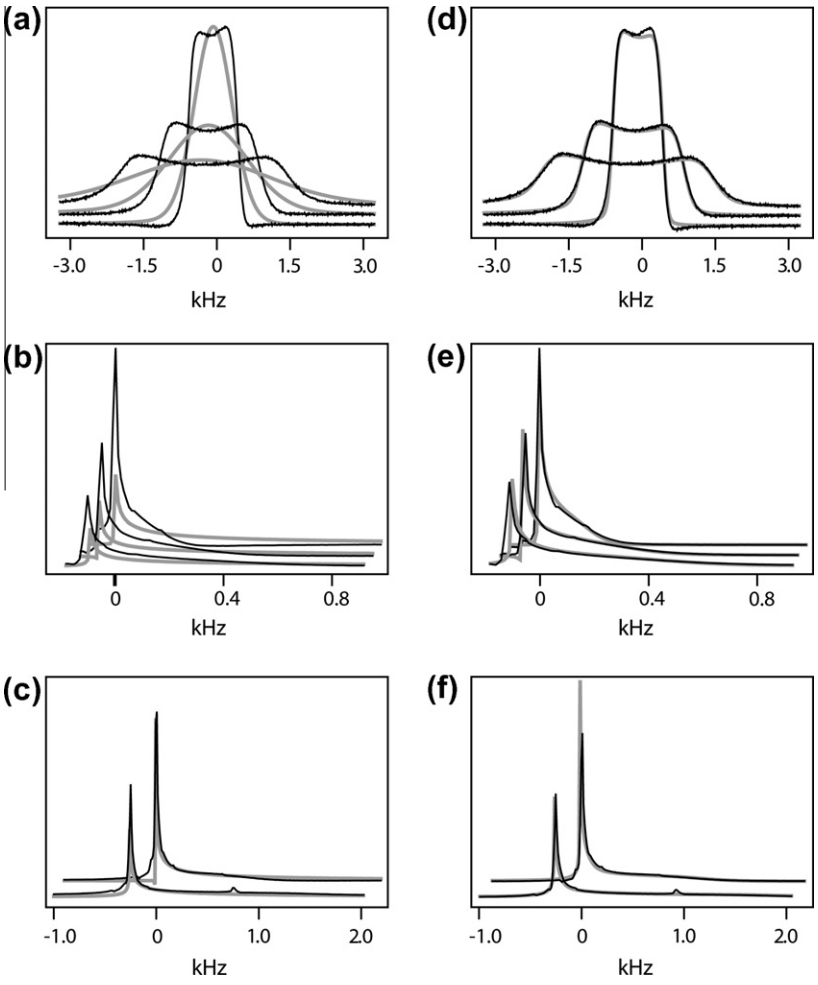

Fig. 1. Comparison of experimental one dimensional images for water shown as the solid black lines to the results of the single Gaussian (a–c) and the Gaussian wave packet (d–f) trial functions shown as the light gray lines. The experimental images of increasing width shown in (a) and (d) respectively correspond to the application of a 1.4 G/cm, 2.8 G/cm, and 4.5 G/cm constant field gradient applied to a 5 cm long sample contained in a 1.6 cm long rf coil. The experimental images of increasing vertical offset shown in (b) and (e) respectively correspond to the application of 18.8 G/cm^2, 12.5 G/cm^2, and 6.4 G/cm^2 and quadratic magnetic fields to the same sample. The lower images shown in (c) and (f) respectively correspond to the application of 2.8 G/cm and 18.8 G/cm^2 and magnetic field variations while the upper images respectively correspond to the application of 1.4 G/cm and 12.5 G/cm^2 linear and quadratic magnetic fields. The ordinates in all of these plots correspond to $M(\omega)/M_0$.

in Fig. 1d–f with the important exception that the signal is calculated from the Gaussian wave packet trial magnetization $M_+^{wp}(\{\xi_2(z_n,t)\})$ constructed from 65 Gaussian basis functions $m_+(\{\xi_2(z_q,t)\})$ and the

$$\xi_0(z_q,0)=\frac{1}{(1+e^{-(z_q-L_0/2)^2/\eta})(1+e^{-(z_q+L_0/2)^2/\eta})} \tag{25}$$

$\xi_1(z_q,0)=0$, and $\xi_2(z_q,0)=500\,\mathrm{cm}^{-2}$ values. The full width at half maximum $L_0=1.9$ cm and the slope $\eta=0.1$ cm of the edges of logistic function product in Eq. (25) were estimated by moving a droplet of water along the z axis through the rf coil. In terms of each $m_+(\{\xi_2(z_q,t)\})$, the $\xi_0(z_q,0)$ value determined from Eq. (25) is a scalar that is used to define $m_+(\{\xi_2(z_q,t)\})$ at $t=0$. Calculation of the spin echo envelope signals for exactly the same conditions yields the solid and dashed light gray lines in Figs. 2a–c and d–f for the single Gaussian $M_+^G(\{\xi_2(2\tau)\})$ and the Gaussian wave packet $M_+^{wp}(\{\xi_2(z_n,2\tau)\})$ trial magnetizations respectively.

5. Discussion

The central theme of this manuscript is to demonstrate a simple NMR application of the time dependent variation of parameters approach pioneered by Dirac, Frenkel, and McLachlan that approximately, and in the cases considered here, solves the Bloch equation. As mentioned in Section 1, the DFM approach generates many if not all of the time dependent approaches to solving the time dependent Schrödinger equation, the Liouville von Neumann equation, or the Bloch equation familiar to NMR spectroscopists. Straightforward examples include the eigenvalue solution $|\psi(t)\rangle=\sum_n \exp(-iE_nt)|\psi_n(0)\rangle$ and Floquet's solution $|\psi(t)\rangle=\sum_n a_n(t)\exp(-in\omega t)|\psi_n(0)\rangle$ with the variable parameters $a_n(t)$ respectively applied when either a time independent Hamiltonian with eigenvalues E_n and eigenfunctions $|\psi_n\rangle$ or a time dependent Hamiltonian oscillating at frequency ω are encountered. The strength of the DFM variation of parameters approach in comparison to the customary methods to solving time dependent problems is flexibility. The approach does not *a priori* require a specific form for the wave function, density operator, or magnetization as the machinery used to develop and test the optimum parameter values is independent of the function choice. The actual values of the variation parameters $\{\xi_n(t)\}$ do depend on the trial function choice and trial function selection can be motivated by the time dependence of measured data.

The approach provides an interesting bridge between experiment and theory where one typically compares raw experimental

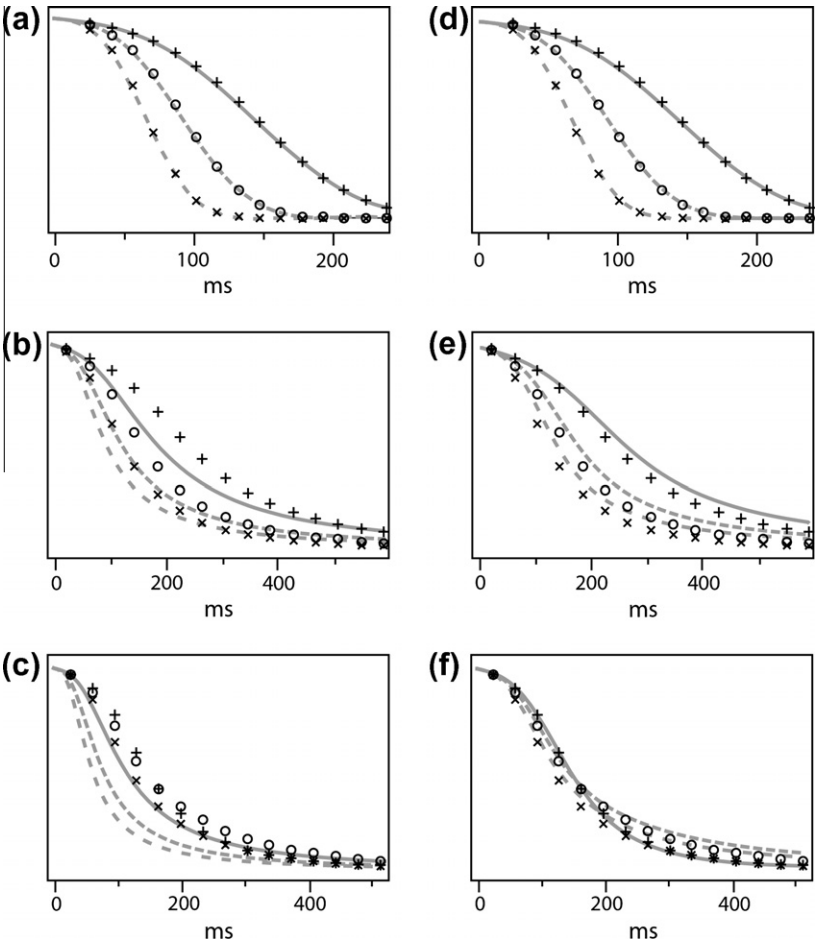

Fig. 2. Comparison of experimental spin echo envelope signals for water shown as the black symbols to the results of the single Gaussian (a–c) and the Gaussian wave packet (d–f) trial functions shown as the light gray lines. The experimental spin echo envelope signals corresponding to the cross, open circle, and x symbols in (a) and (d) respectively correspond to the application of 1.4 G/cm, 2.8 G/cm, and 4.5 G/cm constant gradients applied to a 5 cm long sample contained in a 1.6 cm long rf coil. The experimental spin echo envelope signals corresponding to the cross, open circle, and x symbols in (b) and (e) respectively correspond to the application of 6.4 G/cm^2, 12.5 G/cm^2, and 18.8 G/cm^2 quadratic magnetic fields to the same sample. The echo envelope signals shown in (c) and (f) all correspond to the application of a 1.4 G/cm constant magnetic field gradient while the value of the linear gradient increases as 6.4 G/cm^2, 12.5 G/cm^2, and 18.8 G/cm^2 for the cross, open circle and x symbol respectively. The ordinates in all of these plots correspond to $M(t)/M_0$.

data to direct analytical or numerical simulations. This is a rather challenging prospect when many spins are involved, nonlinear couplings between spins are present, or time dependent processes in solids such as magic angle spinning, decoupling, or cross polarization exist. Instead of such a direct comparison between experiment and theory, a subset of time dependent solutions to the problem can be considered by allowing the measured data to guide trial function selection in terms of $n+1$ variation parameters $\{\xi_n(t)\}$. The optimum values of these $n+1$ parameters according to the DFM approach essentially corresponds to fitting the trial function to theory.

The effects of molecular diffusion on one dimensional images and spin echo envelope signals in applied linear and quadratic shaped magnetic fields were chosen as an experimental platform for demonstrating the application of the DFM variational approach to NMR problems for three reasons. The effects of molecular motion on simple images and spin echo envelope signals in constant gradients are well known, the simple Bloch decay and spin echo pulse sequences and associated changes in the z1 and z2 shims can be performed on any high resolution liquid state pulsed NMR instrument, and the theoretical approach can, in most cases, be completed by hand with some help of a desktop computer.

The application of the DFM approach to NMR problems also has computational cost benefits in comparison to a direct numerical simulation. For the example described by Eq. (1) the free induction signal can be iteratively determined at all time points t and spatial positions x, y, and z. In direct analogy, the free induction signal for the magnetization described by Eq. (1) could also be solved iteratively using the DFM approach. However, with the DFM approach, the spatial portion of the magnetization is treated analytically and the only remaining iteration variable is time t. Therefore, the cost benefit of the DFM approach is that a reduced number of numerical simulations must be performed.

A consequence of the choice to analyze measurements from well understood experiments is the ability of the DFM approach to generate classic expressions for measured signals in certain experimental situations. Examples of the calculation of the Bloch decay free precession signal and the recovery of Hahn's famous expression for the spin echo envelope signal for a small sample well within an rf coil are provided in Eqs. (22) and (23). Each of these examples are largely consistent with experimental observations in the case where the physical molecular displacement on the experimental time scale is small with respect to the sample size. Conditions not treated here include a larger diffusion coefficient, smaller sample, or longer experiment time which require that boundary effects be considered. As long as these physically large sample, slow motion limits are experimentally realized, Eq. (22) predicts that the one dimensional image captured by the sinc

function is broadened by both the effects of transverse relaxation and molecular motion via the $-t/T_2$ and $-(\gamma G)^2 Dt^3/3$ terms respectively. Hahn's result in Eq. (23) generated using the DFM method is independent of sample shape as long as homogeneous rf pulses are applied. Here the signal leading to the spin echo reverses phase at the time $t = \tau$ and information relating to the sample shape refocuses at the echo maximum. Hence, the echo envelope decay is related only to transverse relaxation and diffusion.

The analytical aspects of the DFM approach are further demonstrated in Eq. (24) by the free precession signal corresponding a long sample enclosed by a much smaller rf coil. The effects of rf inhomogeneity on coherence excitation and detection are approximated in this expression by choosing a non-zero $\xi_2(0)$ value that defines both the initial small tip angle single Gaussian trial function as $M_+^G(\{\xi_2(0)\}) = \exp(-\xi_2(0)z^2)$ and the rf coil detection profile as $g(z) = M_+^G(\{\xi_2(0)\})$. The Gaussian rf detection profile is included in Eq. (24) as the quadratic time dependent term in the exponential while the familiar linear and cubic time dependent terms capture the effects of relaxation and diffusion respectively. The cubic diffusion terms in Eqs. (22) and (24) differ by a factor of four. The difference in these two equation stems from the difference in the excitation and detection profile applied to each trial magnetization. The excitation profile for the free precession signal in Eq. (22) is a flat, homogenous function whereas the excitation profile used to generate Eq. (24) is Gaussian. This Gaussian excitation reduces the effect of diffusion as the entire sample is not excited uniformly leading to the factor of four attenuation in the cubic term in Eq. (24) in comparison to Eq. (22).

These special cases of the Bloch decay free precession signals for a restricted volume sample and an infinitely long sample with Gaussian excitation and detection as well as the spin echo envelope signal for the restricted volume sample capture the analytical aspects of the DFM approach. However, for most experimental situations where linear and quadratic shaped magnetic fields are applied to long samples with non-Gaussian rf excitation and detection profiles where the Gaussian wave packet solutions to the Bloch Eq. (7) apply, the sheer number of variational parameters is so large that reporting analytical solutions is not possible given limited space. Therefore numerical solutions to Eqs. (12) and (8) are used to compare to experiment.

Comparison of the theoretical results shown in Fig. 1d–f indicates that the Gaussian wave packet trial function provides a far superior match to the experimental data than the single Gaussian trial function. The source of the failure of the single Gaussian trial function to reliably reproduce experimental data is seen by comparing Fig. 1a and d and by acknowledging the results of rf field mapping. Here the small 1.6 cm long rf coil surrounding the 5 cm long sample does not deliver a homogeneous $\pi/2$ rf pulse to the entire sample. Instead, the magnetization at the coil edges experiences a diminished tip angle and coupling this with an applied linear magnetic field variation leads to the one dimensional box like images in Fig. 1a and d. Therefore to a crude level of approximation, the experimentally obtained images in Fig. 1a and d report on the shape of the rf field. In the case of the single Gaussian trial function the shape of the initial magnetization distribution $M_+^G(\{\xi_2(0)\}) = \exp(-\xi_2(0)z^2)$ can only ever be Gaussian. This function is not consistent with the actual rf excitation profile determined by translating a droplet of water through the rf coil. The results of the Gaussian wave packet analysis in Fig. 1d for applied linear fields provide a much better agreement with experiment. The consequence of the rf field profile on the quadratic shaped magnetic field images in Fig. 1b and e are different than in the case of the standard linear shaped magnetic field images shown in Fig. 1a and d. It is the linear relationship between measured frequency and position as $\omega = \gamma Gz$ provided by the $z1$ shim that makes analysis of Fig. 1a and d straightforward as the spectral intensity is flat, i.e. $I(\omega) \propto$ constant. The quadratic relationship between measured frequency and position as $\omega = \gamma Kz^2$ leads to a shaped distribution $I(\omega) \propto (\gamma K\omega)^{-1/2}$. This means that the center of the sample at $z = \omega = 0$ creates an infinite intensity singularity that drops to zero as a function of $(\omega)^{-1/2}$ seen in Fig. 1b and e. The primary difference between the single Gaussian and Gaussian wave packet trial function results in these figures respectively occurs at large frequency ω. The effect of finite rf coil length that produced the box like z1 based images in Fig. 1a and d, or essentially a spectrum that probes just a fraction of the sample, causes the $z2$ image to drop to zero at the frequency corresponding to the edge of the rf excitation region. This effect is captured by the Gaussian wave packet trial function in Fig. 1e using the product of logistic functions shown in Eq. (25) that corrects for an imperfect rf excitation profile. The single Gaussian trial function does not recover this "perpendicular" high frequency singularity as the initial Gaussian magnetization distribution is a poor model for actual experiments. A similar good agreement between experiment and theory for the single Gaussian versus the Gaussian wave packet trial functions is observed in the mixed linear and quadratic field cases shown in Fig. 1c and f.

The ability of the Gaussian wave packet trial function to reproduce simple one dimensional images in linear and quadratic shaped magnetic fields and the corresponding poor performance of the single Gaussian trial function persists in the analysis of the spin echo envelope signals as shown in Fig. 2. Again, the failure of the single Gaussian trial function to reproduce experimental spin echo envelope signals is due to the simple fact that the experimental rf excitation and detection profiles are not Gaussian. The initial width of the single Gaussian trial function was chosen to be identical to those used to generate the free precession signals in Fig. 1a and b. The simulated spin echo envelope signals shown in Fig. 2b have smaller T_2 values for larger applied gradients than the measured data suggesting that the single Gaussian trial function does not reliably reproduce the measured dynamics for the application of quadratic shaped fields. On the other hand, the Gaussian wave packet trial function naturally incorporating the appropriate rf field profile does remarkably well at reproducing experiment using the appropriate T_2 value measured for water as shown in Fig. 2d–f.

Although the Gaussian wave packet trial function is computationally more intensive than the single Gaussian, the Gaussian wave packet more effectively reproduces experiment. The Gaussian wave packet trial function only begins to deviate from measured data at large quadratic field values. This discrepancy between experiment and the Gaussian wave packet generated results is likely due to a primitive handling of the rf pulse excitation. In the case of a single rf pulse the excitation is taken to correspond to an initial rf profile neglecting any effects of gradient induced offset frequencies. In actuality, an rf field applied in the $\hat{x}$ direction with a spatially dependent Rabi frequency $\omega_1(z)$ does not simply rotate z magnetization in the y–z plane; this approximation changes the size of magnetization along the $\hat{z}$ and $\hat{y}$ axes. Rather, the initial z magnetization rotates around an effective field $[\omega_1(z)^2 + (\gamma Gz + \gamma Kz^2)^2]^{1/2}$ to yield transverse magnetization distributed in the x-y plane. The incorrect handling of the initial rf pulse has little effect on the one dimensional images as the phase deviation away from the expected $\hat{y}$ axis only occurs at the edge of the rf coil for large z values. These isochromats provide a limited contribution to the measured signal or one dimensional image. Application of a second rf pulse, that again reflects the direction of the effective field, to generate the spin echo envelope signal can in principal compound the disagreement between experiment and theory. It may be that it is this effect that leads to the discrepancy between the Gaussian wave packet trial function predictions and experiment at high quadratic field values. Another more likely possibility for this high K

value disagreement revolves around the implementation of the operation prescribed by Eq. (19). The set of known parameters $\{\xi_2(z_n,\tau)\}$ constituting $M_{\pm}^{wp}(\{\xi_2(z_n,\tau)\})$ immediately before the π rf pulse of the spin echo pulse sequence are used to generate the new set of parameters $\{\xi_2(z_n, 0_+)\}$ comprising $M_{\pm}^{wp}(\{\xi_2(z_n,0_+)\})$ at the time $t = 0_+$ immediately after the π rf pulse. The parameter sets before $\{\xi_2(z_n, \tau)\}$ and after $\{\xi_2(z_n, 0_+)\}$ the π rf pulse are related by the rf pulse tip angle taken to be $2\theta(z) = \pi$ at $z = 0$. Even in the limit considered here where the effective field direction is neglected, the only way to relate the two parameter sets is to fit the Gaussian trial function $M_{+}^{wp}(\{\xi_2(z_n,0_+)\})$ to the $2\theta(z)$ weighted mixture of the Gaussian wave packet trial functions $M_{\pm}^{wp}(\{\xi_2(z_n,\tau)\})$ before the application of the $2\theta(z)$ pulse. A different, more efficient approach was used here. Instead of dealing with the entire Gaussian wave packet $M_{+}^{wp}(\{\xi_2(z_n,0_+)\})$, the approximation that a relationship similar to Eq. (19) exists between the individual Gaussian basis functions $m_+(\{\xi_2(z_q, t)\})$ before at the time $t = \tau$ and after at the time $t = 0_+$. Operation in this way essentially imparts a coarse grain approximation to the spatial effects of the applied rf pulse. Even with this approximation that limits the number of parameters to be related in one equation from $3(n + 1)$ to 3, the actual solution to Eq. (20) still requires that the Gaussian basis function $m_+(\{\xi_2(z_q,0_+)\})$ must be fit to the $2\theta(z)$ weighted mixture of the $m_{\pm}(\{\xi_2(z_q,\tau)\})$ basis functions. An additional simplification that is likely the root of the large K value discrepancy between experiment and theory for the spin echo envelope signal shown in Fig. 2e is that instead of fitting the full Gaussian $m_+(\{\xi_2(z_q,0_+)\})$ trial function to the $2\theta(z)$ weighted sum of Gaussians $m_{\pm}(\{\xi_2(z_q,\tau)\})$, each Gaussian basis function in Eq. (20) was expanded as $m_+(\{\xi_2(z_q,t)\}) = 1-\xi_2(z_q,t)(z-z_q)^2 - \xi_1(z_q,t)(z-z_q) - \xi_0(z_q,t)$. After the $2\theta(z)$ rf pulse, like powers of $(z - z_q)$ were equated to generate three equations to solve for the three unknown parameters $\{\xi_2(z_q,0_+)\}$ in terms of the known parameters $\{\xi_2(z_q,\tau)\}$ before the $2\theta(z)$ rf pulse. This operation will work when $2\theta(z) = \pi$, but for larger rf inhomogeneity and or larger magnetic field gradient values the approximations break down consistent with the results shown in Fig. 2e. One way to improve the agreement between experiment and theory in these large K, or poor rf inhomogeneity situations is to fit either the $m_+(\{\xi_2(z_q, 0_+)\})$ isochromatic function or the full wave packet $M_{\pm}^{wp}(\{\xi_2(z_n,0_+)\})$ to the $t = \tau$ trial function distributions prior to the $2\theta(z)$ rf pulse.

6. Conclusion

The DFM variation of parameters is a useful way to approximately and in some cases exactly solve the time dependent Schrödinger equation. An explanation of how to apply the method to NMR problems was provided and used to model the effects of molecular diffusion on experimentally obtained one dimensional images and spin echo envelope signals. An advantage of this approach includes flexibility in the choice of a functional solution to the magnetization dynamics. Parameterized function choices motivated by experimental data are used to estimate the dynamics defined by these trial functions. The weakness of the method is that it does not provide exact solutions to all time domain problems.

The dynamics of the specific case of molecular diffusion considered here is exactly solved using Heller's Gaussian trial function [17,18]. Superb agreement between experiment and theory is realized by using a Gaussian wave packet trial function to incorporate rf inhomogeneity effects, an approach that only seems to break down for spin echo envelope signals recorded for large quadratic field variations. This deviation between experiment and theory is likely due to an inaccurate incorporation of the effects of π rf pulse inhomogeneity in the calculated spin echo signal.

The DFM approach is completely general and can be applied to any time dependent NMR problem. Current work involves describing the magnetization dynamics for the inhomogeneous radiation damped system. As Gaussian functions are not the best trial function choice for these systems, evaluation of the functional will not necessarily equal zero. Various trial functions are used to calculate three component spin echo signals [22] in symmetric and asymmetric inhomogeneous static magnetic fields. The associated error estimates of the trial functions are determined by evaluation of the functional and its proximity to zero. Other effects amenable to treatment with the DFM variation of parameters include an analytical description of rf gradient diffusion filters applied to molecular systems displaying chemically shifted lines, and a number of challenging solids experiments including decoupling and cross polarization in the presence of high speed magic angle spinning. In these more general purely quantum mechanical problems the application of the DFM variation of parameters is more involved. One approach uses projection operators to first generate a reduced dimension time dependent differential equation for a subspace of the overall spin density operator. These projected differential equations necessarily involve a time dependent convolution integral of a memory function [26] that can be calculated and a functional can be defined in terms of a manageable set of parameterized functions that can be optimized according to the DFM variation of parameters. Coupling this approach to solving purely quantum mechanical problems with the results provided here for a semi-classical example imply that any time dependent phenomena in NMR spectroscopy can be analyzed with the DFM variation of parameters. It is hoped that this work stimulates additional applications in the continually broadening field of NMR spectroscopy.

Acknowledgment

Enlightening conversations with Professor Bill McCurdy are gratefully acknowledged.

References

[1] R.R. Ernst, G. Bodenhausen, A. Wokaun, Principles of Nuclear Magnetic Resonance in One and Two Dimensions, Oxford University Press, USA, 1990.
[2] M. Veshtort, R. Griffin, SPINEVOLUTION: a powerful tool for the simulation of solid and liquid state NMR experiments, J. Magn. Reson. (San Diego, Calif.: 1997) 178 (2006) 248–282.
[3] P. Guntert, N. Schaefer, G. Otting, K. Wuthrich, POMA: a complete mathematica implementation of the NMR product-operator formalism, J. Magn. Reson., Ser. A 101 (1993) 103–105.
[4] M. Cuperlovic, G.H. Meresi, W.E. Palke, J.T. Gerig, Spin relaxation and chemical exchange in NMR simulations, J. Magn. Reson. 142 (2000) 11–23.
[5] F. Bloch, Nuclear induction, Phys. Rev 70 (1946) 460–474.
[6] O.W. Sørensen, G.W. Etch, M.H. Levitt, G. Bodenhausen, Uniform excitation of multiple-quantum coherence: application to multiple quantum filtering, Prog. NMR Spectrosc. 16 (1983) 169.
[7] M.M. Maricq, Application of average Hamiltonian theory to the NMR of solids, Phys. Rev. B 25 (1982) 6622.
[8] M. Leskes, P.K. Madhu, S. Vega, Floquet theory in solid-state nuclear magnetic resonance, Prog. Nucl. Magn. Reson. Spectrosc. 57 (2010) 345–380.
[9] U. Haeberlen, High resolution NMR in solids: selective averaging, Academic Press, 1976.
[10] M. Deschamps, G. Kervern, D. Massiot, G. Pintacuda, L. Emsley, P.J. Grandinetti, Superadiabaticity in magnetic resonance, J. Chem. Phys. 129 (2008) 204110. 204110.
[11] M. Goldman, P.J. Grandinetti, A. Lior, Z. Olejniczak, J.R. Sachleben, Theoretical aspects of higher-order truncations in solid-state nuclear magnetic resonance, J. Chem. Phys 97 (1992) 8947.
[12] M. Leskes, R.S. Thakur, P.K. Madhu, N.D. Kurur, S. Vega, Bimodal Floquet description of heteronuclear dipolar decoupling in solid-state nuclear magnetic resonance, J. Chem. Phys 127 (2007) 024501.
[13] M. Bak, J.T. Rasmussen, N.C. Nielsen, NMR spectroscopy, Journal of Magnetic Resonance 147 (2000) 296–330.
[14] P.A.M. Dirac, Note on exchange phenomena in the Thomas atom, Proc. Camb. phil. Soc 26 (1930) 376.
[15] J. Frenkel, Wave Mechanics, Advanced General Theory,, Clarendon Press, Oxford, 1934.

[16] A.D. McLachlan, A variational solution of the time-dependent Schrodinger equation, Mol. Phys 8 (1964) 39–44.
[17] E.J. Heller, Time-dependent approach to semiclassical dynamics, J. Chem. Phys 62 (1975) 1544.
[18] E.J. Heller, Time dependent variational approach to semiclassical dynamics, J. Chem. Phys 64 (1976) 63.
[19] L. Emsley, Spin diffusion in crystalline solids, in: R.K. Harris, R.E. Wasylishen, M.J. Duer (Eds.), NMR Crystallography, John Wiley & Sons Ltd., 2009.
[20] A.E. Bennett, C.M. Rienstra, M. Auger, K.V. Lakshmi, R.G. Griffin, Heteronuclear decoupling in rotating solids, J. Chem. Phys. 103 (1995) 6951–6958.
[21] E.O. Stejskal, J. Schaefer, J.S. Waugh, Magic-angle spinning and polarization transfer in proton-enhanced NMR, J. Magn. Reson. 28 (1977) 105–112.
[22] M.P. Augustine, Transient properties of radiation damping, Prog. NMR Spectrosc. 40 (2002) 111–150.
[23] S. Leclerc, L. Guendouz, A. Retournard, D. Canet, NMR diffusion measurements under chemical exchange between sites involving a large chemical shift difference, Concepts Magn. Reson. Part A 36A (2010) 127–137.
[24] E.L. Hahn, Spin echoes, Phys. Rev. 80 (1950) 580.
[25] H.C. Torrey, Bloch equations with diffusion terms, Phys.Rev. 104 (1956) 563.
[26] M. Mehring, Principles of High Resolution NMR in Solids, Springer, Heidelberg, 1983.